Research Paper

Shifting the linear range of the calibration curves for the quantification of oral molecular-targeted anticancer drugs and the active metabolite in human plasma using LC-ESI-MS/MS

Tensei Hirasawa[1], Masafumi Kikuchi[1,2]*, Shinya Takasaki[2], Masaki Kumondai[2], Yu Sato[2], Toshihiro Sato[2], Eishi Imoto[3], Yoshihiro Hayakawa[3], Masamitsu Maekawa[1,2], Nariyasu Mano[1,2]

[1]Faculty of Pharmaceutical Sciences, Tohoku University, 6−3 Aoba, Aramaki, Aoba-ku, Sendai 980−8578, Japan
[2]Department of Pharmaceutical Sciences, Tohoku University Hospital, Seiryo-machi, Aoba-ku, Sendai 980−8574, Japan
[3]Shimadzu Corporation, 1 Nishinokyo Kuwabara-cho, Nakagyo-ku, Kyoto 604−8511, Japan

Abstract Many types of oral kinase inhibitors, including imatinib and gefitinib, have become clinically available and have significantly contributed to improving the survival outcomes in cancer patients. Therapeutic drug monitoring of some oral kinase inhibitors is important for ensuring the efficacy and safety of these drugs. Liquid chromatography-electrospray ionization tandem mass spectrometry (LC-ESI-MS/MS) has been used for the simultaneous quantification of these drugs in the human plasma. However, the development of a simultaneous LC-MS/MS analytical method is difficult owing to the differences in mass spectrometry (MS) sensitivity and the therapeutic range of each drug. In this study, we investigated the linear range shifts of calibration curves by adjusting the collision energy defect, in-source collision-induced dissociation, secondary product ion selected reaction monitoring, and isotopologue selected reaction monitoring to develop a simultaneous quantification method for 20 oral kinase inhibitors and active metabolite of sunitinib. Although these four techniques could easily adjust the number of ions introduced to the MS when used individually, it was difficult to adapt 21 analytes using only one technique. Therefore, it is important to utilize multiple techniques, considering the therapeutic concentration range of each drug, in order to develop a method for the simultaneous quantification of oral kinase inhibitors and active metabolites in molecular-targeted therapy.

Key words: oral kinase inhibitor, LC-ESI-MS/MS, collision energy, in-source collision-induced dissociation, simultaneous quantification

Introduction

Molecular-targeted therapy is an essential treatment for cancer, which targets a specific molecule and controls its function. Many types of oral kinase inhibitors have become clinically available and have contributed significantly to improving the survival outcomes in cancer patients[1,2]. Gefitinib, erlotinib, osimertinib, dacomitinib, lapatinib, and afatinib have been used in patients with non-small cell lung cancer or breast cancer targeting mutations in the ErbB family. Bosutinib, imatinib, dasatinib, nilotinib, and ponatinib are used to treat leukemia by inhibiting BCR-ABL activity. Axitinib and ibrutinib exert their effects by inhibiting the vascular endothelial growth factor receptor and Bruton's tyrosine kinase, respectively. In recent years, the use of multikinase inhibitors that inhibit multiple tyrosine kinases such as pazopanib, sorafenib, sunitinib, lenvatinib, vandetanib, regorafenib, and nintedanib, has also increased. Dose reduction and the temporal or persistent discontinuation of drugs are required due to serious side effects caused

* **Corresponding author**
Masafumi Kikuchi
Faculty of Pharmaceutical Sciences, Tohoku University, 6−3 Aoba, Aramaki, Aoba-ku, Sendai 980−8578, Japan
Tel: +81−22−717−7541, Fax: +81−22−717−7545
E-mail: masafumi.kikuchi.b2@tohoku.ac.jp
Received: December 30, 2021. Accepted: March 24, 2022.
Epub April 26, 2022.
DOI: 10.24508/mms.2022.06.006

by the administration of kinase inhibitors. Furthermore, there are large inter-individual variations in the concentrations of the oral kinase inhibitors in blood, and these concentrations are correlated with therapeutic effects and side effects. Therapeutic drug monitoring (TDM) of oral kinase inhibitors has been reported to be useful for improving their therapeutic effects[3,4]. Therefore, a consideration of the concentration of the oral kinase inhibitors is important for ensuring the efficacy and safety of these drugs[5–10]. In addition, cancer patients often have multiple therapeutic targets and may be combined with oral kinase inhibitors. Due to the importance of administration design based on blood levels of many oral kinase inhibitors, a rapid simultaneous measurement system is required in clinical practice.

Many methods have been reported for the quantification of drug concentrations in human plasma using liquid chromatography-electrospray ionization tandem mass spectrometry (LC-ESI-MS/MS)[11–13]. Altering the measurement conditions for analyzing a patient sample requires considerable time and effort, and the efficiency of the routine of TDM is significantly reduced. Therefore, a method for the simultaneous evaluation of the oral kinase inhibitors is required. However, both the therapeutic range and linearity of the calibration curve must be considered when designing a simultaneous LC-ESI-MS/MS method. Therapeutic ranges for every drug vary with differences in their pharmacokinetic and pharmacodynamic parameters. In fact, the therapeutic concentration range of ibrutinib (0.3−300 ng/mL) and pazopanib (30−50,000 ng/mL) varies more than 100,000 times.

In addition, the linearity range of the calibration curve for each drug was specified using its physicochemical properties based on the chemical structure. Previously, we demonstrated the utility of the linear range shift technique using in-source collision-induced dissociation (CID), which can be used for the simultaneous analysis of the concentrations of drugs and their metabolites with different calibration curve ranges[14–18]. The linear range shift of the calibration curves was investigated by adjusting the following parameters: collision energy defect (CED), which shifts the collision energy (CE) from the optimized value[19]; secondary product ion selected reaction monitoring (*s*-SRM), which selects low-intensity product ions[20]; and isotopologue SRM (*i*-SRM), which sets precursor and product ions to those containing isotope atoms[21](Fig. 1).

In this study, we investigated whether the linear range shifts by adjusting CED, in-source CID, *s*-SRM, and *i*-SRM for the measurement of the plasma concentration of 20 oral kinase inhibitors and active metabolite of sunitinib: afatinib, axitinib, bosutinib, dacomitinib, dasatinib, erlotinib, gefitinib, ibrutinib, imatinib, lapatinib, lenvatinib, nilotinib, nintedanib, osimertinib, pazopanib, ponatinib, regorafenib, sorafenib, sunitinib, *N*-desethyl sunitinib, and vandetanib (Fig. 2).

Materials and Methods

Chemical and reagents

Afatinib, bosutinib, dacomitinib, gefitinib, ibrutinib, imatinib, lapatinib, lenvatinib, nilotinib, nintedanib, osimertinib, ponatinib, regorafenib, vandetanib, afatinib-$^{2}H_{6}$ (internal standard (IS)), bosutinib-$^{2}H_{8}$, dasatinib-$^{2}H_{8}$, gefitinib-$^{2}H_{6}$, ibrutinib-$^{2}H_{5}$, lapatinib-$^{2}H_{4}$, nilotinib-$^{2}H_{6}$, nintedanib-^{13}C-$^{2}H_{3}$, and pazopanib-$^{2}H_{6}$ were purchased from Cayman Chemical Company (Ann Arbor, MI). Axitinib, erlotinib, sorafenib, sunitinib, *N*-desethyl sunitinib, axitinib-$^{2}H_{3}$, erlotinib-$^{2}H_{6}$, Imatinib-$^{2}H_{8}$, sorafenib-$^{2}H_{3}$, and sunitinib-$^{2}H_{4}$ were purchased from Toronto Research Chemicals (Toronto, Canada). Dasatinib was purchased from LC Laboratories (Woburn, MA). Dacomitinib-$^{2}H_{10}$, lenvatinib-$^{2}H_{5}$, osimertinib-^{13}C-$^{2}H_{3}$, ponatinib-$^{2}H_{8}$, regorafenib-^{13}C-$^{2}H_{3}$, and vandetan-

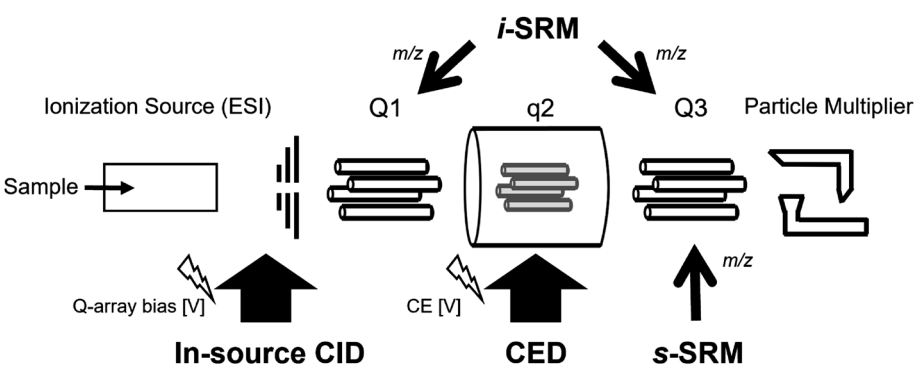

Fig. 1. Ion abundance adjustment method in LC/ESI-MS/MS.

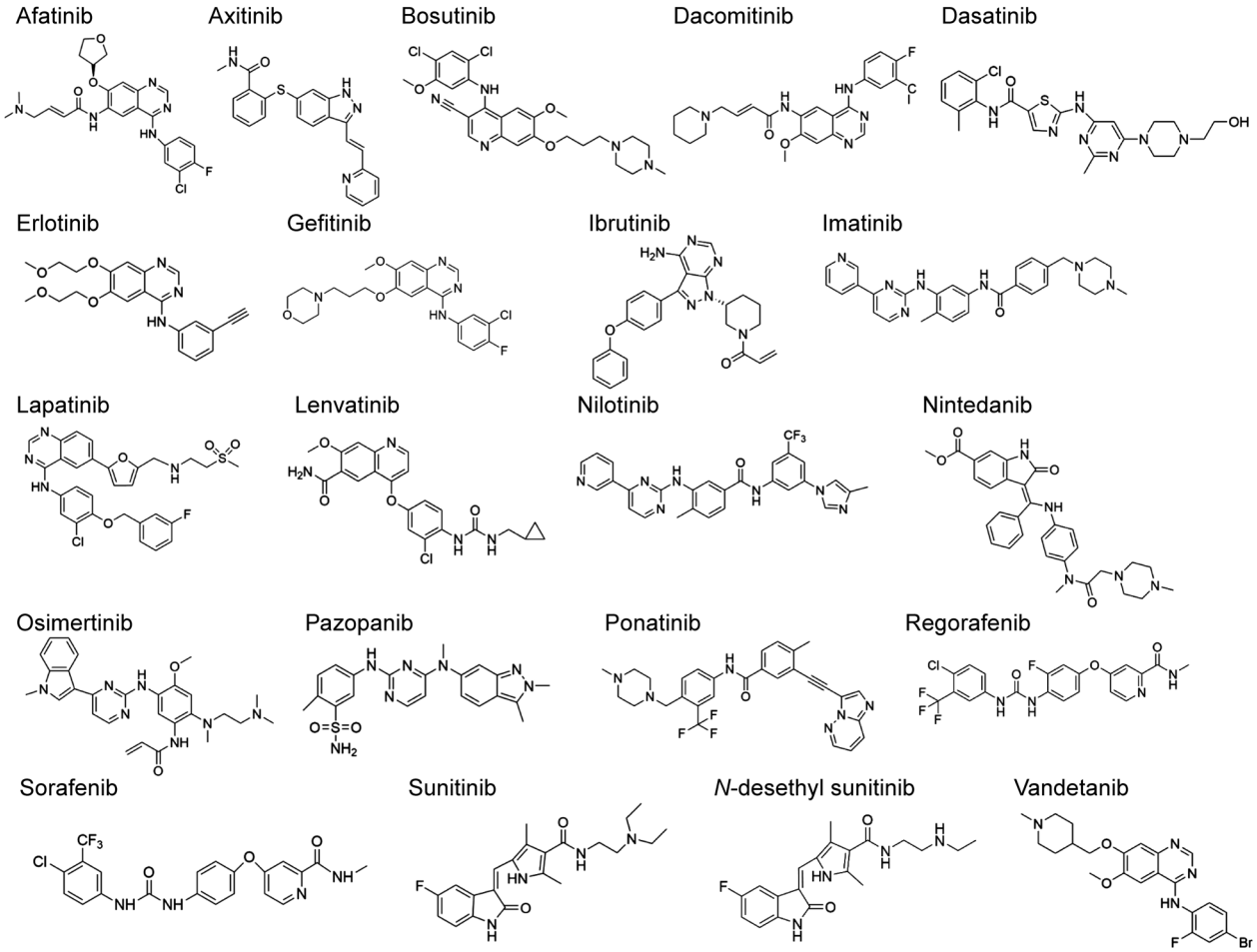

Fig. 2. Chemical structures of afatinib, axitinib, bosutinib, dacomitinib, dasatinib, erlotinib, gefitinib, ibrutinib, imatinib, lapatinib, lenvatinib, nilotinib, nintedanib, osimertinib, pazopanib, ponatinib, regorafenib, sorafenib, sunitinib, *N*-desethyl sunitinib, and vandetanib.

ib-^{13}C-$^{2}H_6$ were purchased from Alsachim (Illkirch-Graffenstaden, France). Pazopanib was purchased from Synkinase (Melbourne, Victoria, Australia). High performance liquid chromatography (HPLC)-grade ammonium formate, formic acid, and methanol were purchased from the Fujifilm Wako Pure Chemical Corporation (Osaka, Japan). HPLC-grade acetonitrile was purchased from the Kanto Chemical Corporation (Tokyo, Japan). Ultrapure water was prepared using a Puric-α apparatus and was used for the LC-ESI-MS/MS analysis. All other chemicals used were of the highest commercially available purity. Heparinized human plasma was supplied by Cosmo Bio Co. Ltd. (Tokyo, Japan).

Preparation of calibration standards and IS solutions

Each calibration standard was prepared by diluting the stock solutions to 0.1, 0.3, 1.0, 3.0, 10, 30, 100, 300, 1,000, 3,000, and 10,000 ng/mL in plasma. Calibration standards were stored at −80°C in light-protected containers. Each IS solution was prepared by diluting the stock solutions to 100 ng/mL in acetonitrile-methanol (9 : 1, v/v).

Sample pre-treatment

Eighty microliters each of IS and acetonitrile-methanol (9 : 1, v/v) solution were added to 40 μL of the plasma sample contained in a 1.5 mL microcentrifuge tube. The mixture was vortexed for 5 min and centrifuged at 14,000 × *g* for 10 min. After centrifugation, 2 μL of supernatant was injected into the analytical system.

LC-ESI-MS/MS conditions

The LC-ESI-MS/MS analysis was performed using an LCMS-8050 triple quadrupole mass spectrometer coupled with a Nexera X2 UHPLC system (Shimadzu, Kyoto, Japan). All data acquisition and processing was performed using LabSolutions (Shimadzu). The Nexera X2 UHPLC system consisted of a vacuum degasser, two solvent deliv-

ery systems, an autosampler, and a column oven. Chromatographic separation was achieved using a YMC-Triart C18 metal-free column (2.1 mm i.d. × 50 mm, 3 μm; YMC, Kyoto, Japan). The column temperature was maintained at 40˚C, and the samples were kept at 4˚C. The flow rate was set at 0.45 mL/min, and the injection volume was 2 μL for analysis. Mobile phases A and B comprised 10 mM aqueous ammonium formate (A) adjusted to pH 3.6 and 10 mM of ammonium formate-methanol (B). The gradient program was as follows: elution was initiated with 5% B, followed by a linear gradient to 100% B in 1 to 3 min, held at 100% B for 1 min, and then immediately returned to the initial conditions, which were maintained for 1 min until the end of the run. The LCMS-8050 was equipped with an ESI source operating in the positive-ion detection mode. The conditions for mass spectrometry (MS) analysis were as follows: probe voltage, 4,000 V; desolvation line temperature, 250˚C; block heater temperature, 400˚C; interface temperature, 300˚C; nebulizing gas flow, 3 L/min; drying gas, 10 L/min; and heating gas flow, 10 L/min. Table 1 summarizes the optimized SRM conditions for each analyte.

CED

The collision energy was changed from −5 to −50 V under the optimized SRM conditions, and the peak intensities of each 10 pg analyte were plotted against voltages. Triplicate analyses were performed for every voltage for all analytes.

In-source CID

The Q-array bias in SRM analyses was changed from 0 to 180 V under the optimized SRM conditions, and the peak intensities of each 10 pg analyte were plotted against voltages. Triplicate analyses were performed for each voltage for all analytes. Although the Q-array bias could be set to 240 V, the upper limit was set to 180 V because the reproducibility deteriorated at high voltages.

s-SRM

Three product ions with higher peak intensities obtained by a product-ion scan during the optimization of ESI-MS/MS conditions were selected, and the optimum voltage value was set for each analyte (data not shown). The product ions in SRM analyses were changed under optimized SRM conditions, and the peak intensities of each 10 pg ana-

Table 1. Optimized SRM conditions

Analyte	SRM Transitions	CE [V]	Q1 pre bias [V]	Q3 pre bias [V]	Internal standard
Afatinib	486.0>371.2	−29	−10	−18	Afatinib-$^{2}H_{6}$
Axitinib	387.1>356.1	−20	−23	−27	Axitinib-$^{2}H_{3}$
Bosutinib	530.1>141.3	−24	−10	−28	Bosutinib-$^{2}H_{8}$
Dacomitinib	470.0>385.1	−27	−8	−14	Dacomitinib-$^{2}H_{10}$
Dasatinib	488.0>401.2	−29	−6	−30	Dasatinib-$^{2}H_{8}$
Erlotinib	394.1>278.2	−35	−14	−30	Erlotinib-$^{2}H_{6}$
Gefitinib	447.2>128.2	−25	−5	−22	Gefitinib-$^{2}H_{6}$
Ibrutinib	442.1>138.3	−27	−22	−28	Ibrutinib-$^{2}H_{5}$
Imatinib	494.1>394.3	−28	−12	−28	Imatinib-$^{2}H_{8}$
Lapatinib	581.0>365.2	−39	−20	−26	Lapatinib-$^{2}H_{4}$
Lenvatinib	427.1>370.1	−31	−16	−18	Lenvatinib-$^{2}H_{5}$
Nilotinib	530.1>289.3	−32	−5	−20	Nilotinib-$^{2}H_{6}$
Nintedanib	540.1>113.3	−26	−16	−46	Nintedanib-^{13}C-$^{2}H_{3}$
Osimertinib	500.2>72.2	−28	−10	−12	Osimertinib-^{13}C-$^{2}H_{3}$
Pazopanib	438.2>341.4	−48	−28	−16	Pazopanib-$^{2}H_{6}$
Ponatinib	533.2>260.1	−31	−8	−46	Ponatinib-$^{2}H_{8}$,
Regorafenib	483.1>270.2	−33	−14	−28	Regorafenib-^{13}C-$^{2}H_{3}$
Sorafenib	465.1>252.2	−30	−5	−12	Sorafenib-$^{2}H_{3}$
Sunitinib	399.4>283.3	−25	−26	−30	Sunitinib-$^{2}H_{4}$
N-Desethyl Sunitinib	370.9>283.1	−22	−46	−50	Sunitinib-$^{2}H_{4}$
Vandetanib	475.2>112.2	−22	−14	−12	Vandetanib-^{13}C-$^{2}H_{6}$

SRM, selected reaction monitoring; CE, collision energy.

lyte were plotted against *m/z*. Triplicate analyses were performed for each product ion for all analytes.

i-SRM

Isotopologue transitions were selected from the optimized SRM transitions, and the SRM conditions were optimized for each transition (data not shown). The isotopologue transitions in SRM analyses were changed under optimized SRM conditions, and the peak intensities of each 10 pg analyte were plotted against *m/z*. Triplicate analyses were performed for each SRM transition for all analytes.

Linear range shift of calibration curves

According to the previous study of Ishii and Maekawa, we define linear range shift of calibration curves[14,17]. The averages of the triplicates at each calibration standard were used to plot the calibration curves, which were generated using the analyte-to-IS peak area ratios by weighted ($1/x^2$) least squares linear regression. Additional rules for the preparation of the calibration curves were as follows: (1) calibration points with saturated MS intensities were excluded; (2) the lower limits of quantification were set at levels less than 20% of the relative standard deviation; (3) the levels with a relative standard deviation of ＜15% were included as calibration points; (4) the levels within 85−115% of the relative error were used as calibration points; and (5) calibration curves were generated using more than four calibration points.

Results and Discussion

Reduction of the peak intensities and linear range shift of calibration curves by CED

First, we changed the CE parameters affecting the CID of the collision cell and investigated the ion abundance of each analyte. Afatinib showed the maximum intensity at a CE of −29 V. The peak intensities of afatinib gradually decreased as they increased or decreased from the optimized CE value. As a result, the linearity of the calibration curve shifted to the highest concentration range at a CE of −5 V (100−10,000 ng/mL). Axitinib, bosutinib, dacomitinib, dasatinib, erlotinib, gefitinib, ibrutinib, imatinib, lapatinib, lenvatinib, nilotinib, nintedanib, pazopanib, ponatinib, regorafenib, sorafenib, sunitinib, and *N*-desethyl sunitinib showed similar trends to those observed for afatinib. In contrast, osimertinib, which showed the maximum intensity at a CE of −28 V, had relatively little change in ion intensities even at high energies. As a result, the linearity of the calibration curve shifted to a higher concentration range only when excessive energy was applied. In addition, the decrease in ion intensities of vandetanib was also small, the linearity of the calibration curve did not shift to a higher concentration range (Fig. 3 and Table 2).

Considering these results, CED can be widely used regardless of the resolution of MS and the structure of the analytes. However, the effect of CID owing to CE was considered to be less effective when the *m/z* of product ions was small, as seen for osimertinib (*m/z* 72.2) and vandetanib (*m/z* 112.2). Because the product ions of these analytes have already been observed as small fragments, it is expected that further fragmentation will be difficult even if the CE is increased.

Reduction of the peak intensity and linear range shift of calibration curves by in-source CID

Next, the ion abundance of the analytes was investigated by changing the in-source CID conditions. We changed the Q-array bias, which is the ion-guide voltage set immediately after the orifice, and attempted ion reduction to quadrupoles by in-source CID. Although afatinib was stable up to a Q-array bias of 120 V, the ion intensity gradually decreased after 120 V. Consequently, the linearity of the calibration curve shifted to the widest and highest concentration range at Q-array biases of 130 and 140 V (0.3−300 to 3.0−10,000 ng/mL). Bosutinib, dacomitinib, erlotinib, gefitinib, ibrutinib, imatinib, lenvatinib, nintedanib, osimertinib, pazopanib, ponatinib, regorafenib, sorafenib, sunitinib, *N*-desethyl sunitinib, and vandetanib showed similar trends as afatinib. In contrast, dasatinib, lapatinib, and nilotinib were stable against an increase in Q-array bias, and no significant shift in the linearity of the calibration curve was observed (Fig. 4 and Table 2).

Considering these results, in-source CID can be used for most analytes without contaminating MS with excess ions. In addition, the calibration standards for axitinib, imatinib, sorafenib, sunitinib, and *N*-desethyl sunitinib showed similar effects as the in-source CID either with plasma or acetonitrile in their preparation[17]. In contrast, the effect of in-source CID was considered to be less effective for analytes stable to a Q-array bias of 180 V, such as dasatinib, lapatinib, and nilotinib. Although setting the Q-array bias to 190 V or higher may be effective, we considered that the number of ions could not be adjusted by in-source CID for

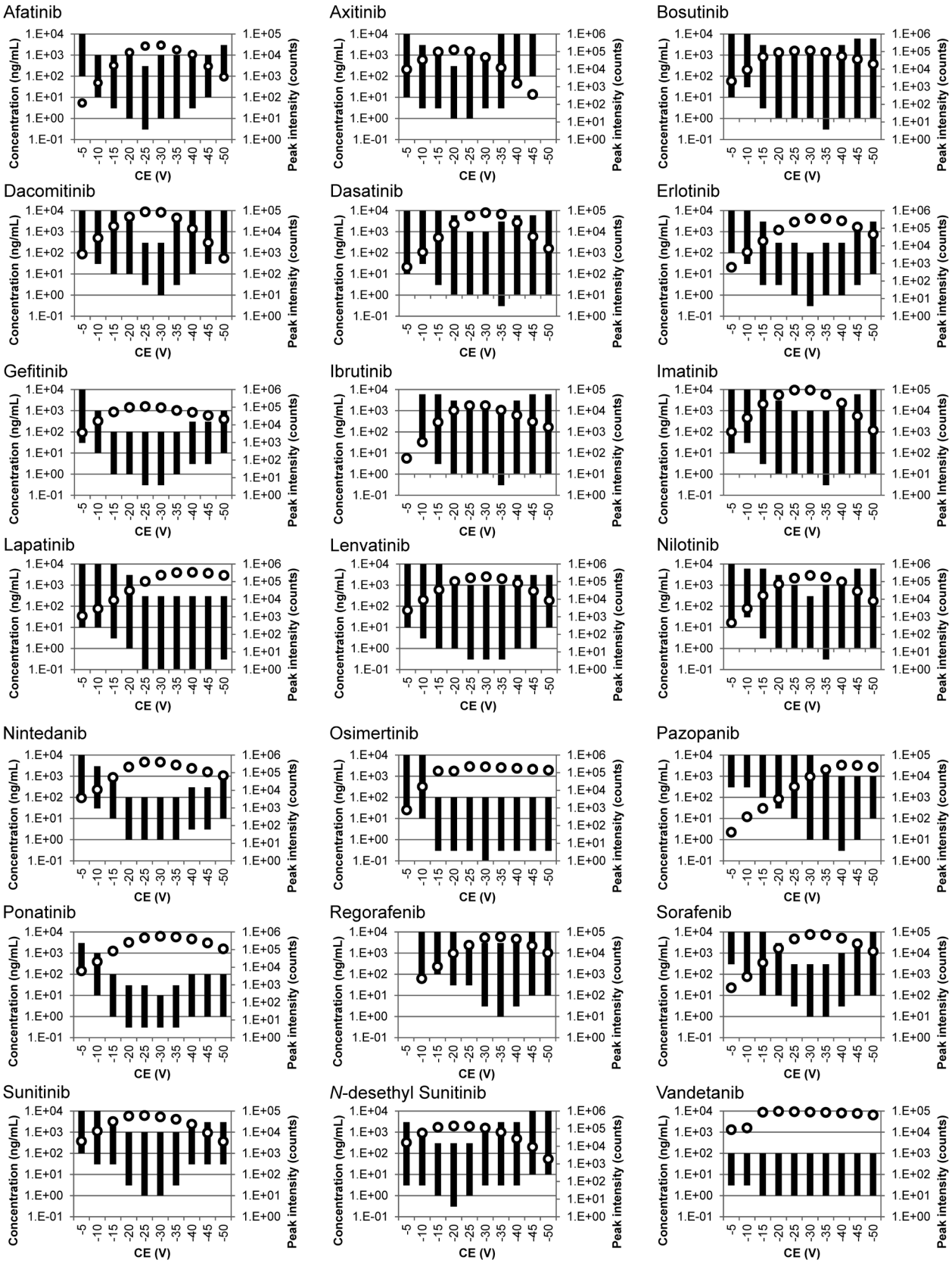

Fig. 3. Peak intensities plot and linearity range of calibration curves for each collision energy value: afatinib, axitinib, bosutinib, dacomitinib, dasatinib, erlotinib, gefitinib, ibrutinib, imatinib, lapatinib, lenvatinib, nilotinib, nintedanib, osimertinib, pazopanib, ponatinib, regorafenib, sorafenib, sunitinib, *N*-desethyl sunitinib, and vandetanib.

The columns represent the linear range of the calibration curves (left *y*-axis). The white dots represent the change in peak intensities of each 10 pg analyte (right *y*-axis).

Table 2. Results of ion adjustment methods for each compound

Compound	CED	IS-CID	*s*-SRM	*i*-SRM
Afatinib	○	○	×	○
Axitinib	○	○	○	○
Bosutinib	○	○	○	○
Dacomitinib	○	○	×	○
Dasatinib	○	×	○	○
Erlotinib	○	○	○	○
Gefitinib	○	○	×	○
Ibrutinib	○	○	○	○
Imatinib	○	○	○	×
Lapatinib	○	×	○	×
Lenvatinib	○	○	○	○
Nilotinib	○	×	○	○
Nintedanib	○	○	×	○
Osimertinib	×	○	○	○
Pazopanib	○	○	○	○
Ponatinib	○	○	○	○
Regorafenib	○	○	○	○
Sorafenib	○	○	○	○
Sunitinib	○	○	○	○
N-Desethyl Sunitinib	○	○	×	○
Vandetanib	×	○	○	○

○, adjustable; ×, not adjustable.

these three analytes because it is difficult to precisely control the Q-array bias under high voltage. In particular, nilotinib has different fragment ions produced by a high Q-array bias and low-energy CID (data not shown). Therefore, it was suggested that the reaction under high pressure with nitrogen gas led to a high threshold of the Q-array bias in the in-source CID.

Reduction of the peak intensity and linear range shift of calibration curves by s-SRM

We then investigated the ion abundance of the analytes under the *s*-SRM conditions. We changed the product ion with the highest ion intensity to one with a relatively lower intensity and investigated the ion abundance of each analyte. Contaminant ions were excluded during analysis, and vandetanib did not contain the corresponding product ions. Three product ions (*m/z* 387.1>356.1, *m/z* 387.1>221.2, and *m/z* 387.1>355.2) were obtained for axtinib, and the ion intensity gradually decreased in transitions at *m/z* 387.1>221.2 and *m/z* 387.1>355.2, compared to the optimized transition *m/z* 387.1>356.1. As a result, the linearity of the calibration curve was obtained in the widest and highest concentration range in the transition at *m/z* 387.1>221.2 (0.1−30 to 1.0−3,000 ng/mL). Bosutinib, dasatinib, erlotinib, ibrutinib, imatinib, lapatinib, nilotinib, osimertinib, pazopanib, ponatinib, regorafenib, sorafenib, sunitinib, and vandetanib showed similar trends to those exhibited by axtinib. In contrast, the ion intensities of afatinib, gefitinib, and *N*-desethyl sunitinib for the secondary product ions (*m/z* 486.0>100.1, *m/z* 447.2>231.2, and *m/z* 370.9>210.5) were very small, and the linearity of their calibration curves shifted to relatively high concentrations in a very narrow range. In addition, the ion intensities of dacomitinib and nintedanib for the secondary product ions (*m/z* 470.0>319.1 and *m/z* 540.1>70.2) were comparable to the optimized transitions, and the linearity of their calibration curves did not shift to the higher concentration range (Fig. 5 and Table 2).

Considering these results, *s*-SRM can be used for various analytes because it is easy to predict the change in peak intensities from the product scan. In contrast, *s*-SRM was considered to be less effective when the intensities of product ions, such as afatinib, gefitinib, *N*-desethyl sunitinib, dacomitinib, and nintedanib, were used.

Reduction of the peak intensity and linear range shift of calibration curves by i-SRM

Finally, we investigated the ion abundance of the analytes under the *i*-SRM conditions. We changed the SRM transition with the highest ion intensity to three isotopologue transitions (*m/z* M_1+1>M_3, *m/z* M_1+1>M_3+1, and *m/z* M_1+2>M_3+2) and investigated the ion abundance of each analyte. Three isotopologue transitions (*m/z* 487.0>371.2, *m/z* 487.0>372.2, and *m/z* 488.0>373.2) were obtained for afatinib, and the ion intensities decreased at all isotopologue transitions compared with the optimized transition *m/z* 386.0>371.2. As a result, the linearity of the calibration curve was obtained in the widest and highest concentration range in the transition at *m/z* 487.0>372.2 (0.3−30 to 1.0−3,000 ng/mL). Axitinib, bosutinib, dasatinib, erlotinib, gefitinib, ibrutinib, lenvatinib, nilotinib, nintedanib, osimertinib, pazopanib, ponatinib, regorafenib, sorafenib, sunitinib, *N*-desethyl sunitinib, and vandetanib showed similar trends as afatinib. In contrast, although the ion intensities of lapatinib at the isotopologue transitions (*m/z* 582.0>365.2, *m/z* 582.0>366.2, and *m/z* 583.0>367.2) and imatinib at the isotopologue transitions (*m/z* 494.1>394.3, *m/z* 495.1>395.3, and *m/z* 496.1>396.3)

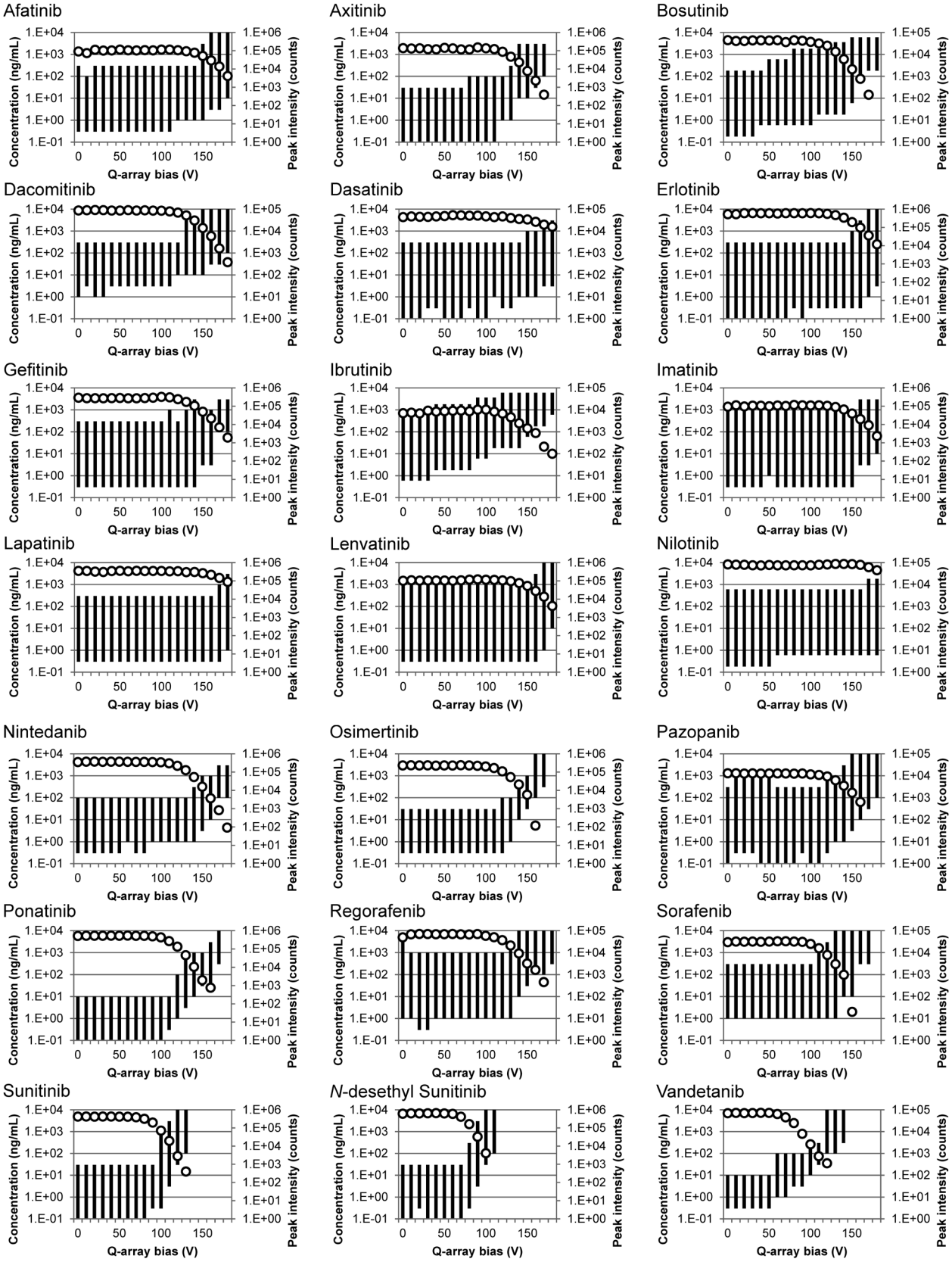

Fig. 4. Peak intensities plot and linearity range of calibration curves for each Q-array bias: afatinib, axitinib, bosutinib, dacomitinib, dasatinib, erlotinib, gefitinib, ibrutinib, imatinib, lapatinib, lenvatinib, nilotinib, nintedanib, osimertinib, pazopanib, ponatinib, regorafenib, sorafenib, sunitinib, *N*-desethyl sunitinib, and vandetanib.

The columns represent the linear range of the calibration curve (left *y*-axis). The white dots represent the change in peak intensities of each 10 pg analyte (right *y*-axis). When the peak intensity was not obtained, the white dot was not described.

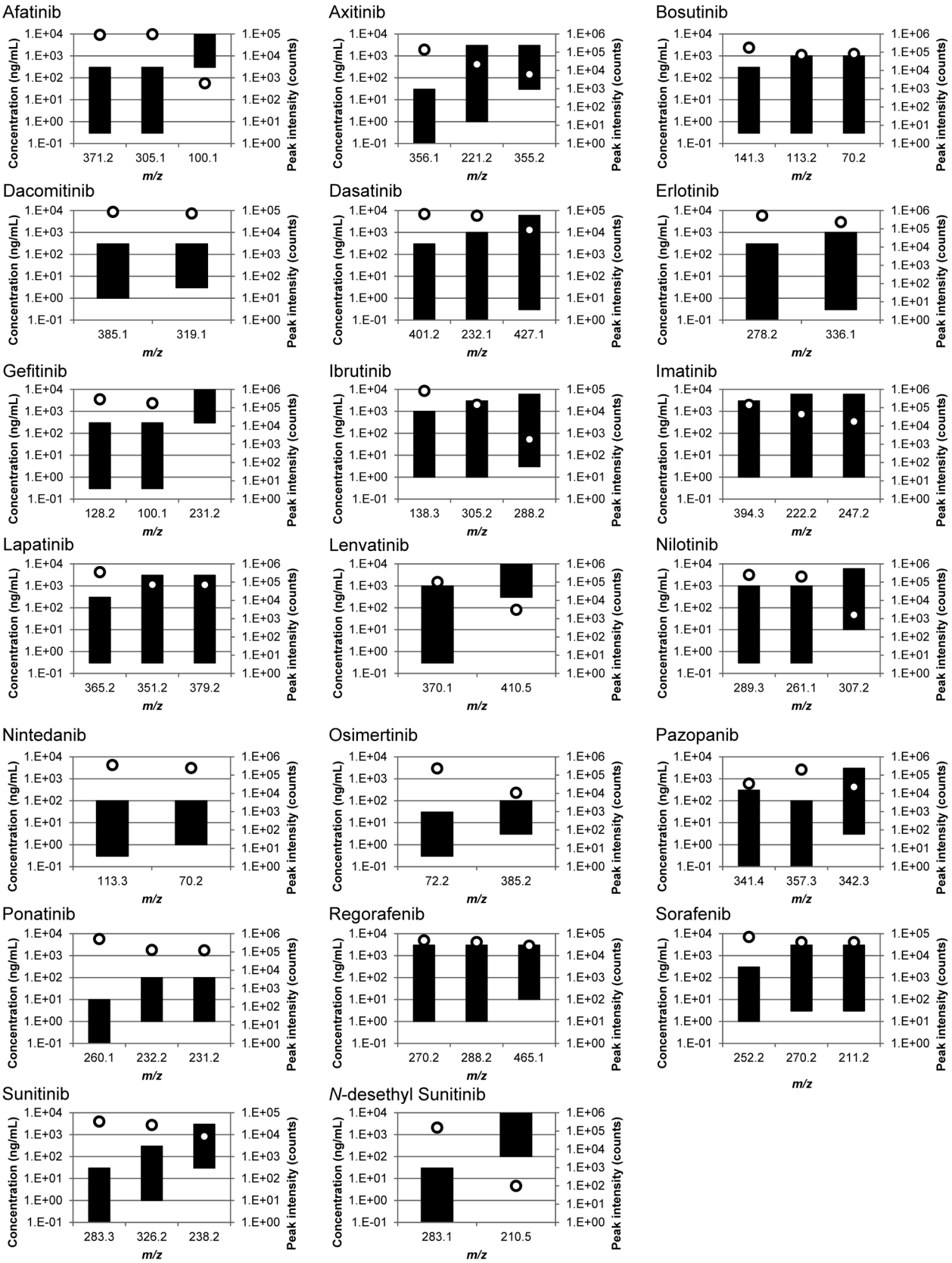

Fig. 5. Peak intensities plot and linearity range of calibration curves for each product ion: afatinib, axitinib, bosutinib, dacomitinib, dasatinib, erlotinib, gefitinib, ibrutinib, imatinib, lapatinib, lenvatinib, nilotinib, nintedanib, osimertinib, pazopanib, ponatinib, regorafenib, sorafenib, sunitinib, and *N*-desethyl sunitinib.

The columns represent the linear range of the calibration curve (left *y*-axis). The white dots represent the change in peak intensities of each 10 pg analyte (right *y*-axis). When the peak intensity was not obtained, the white dot was not described.

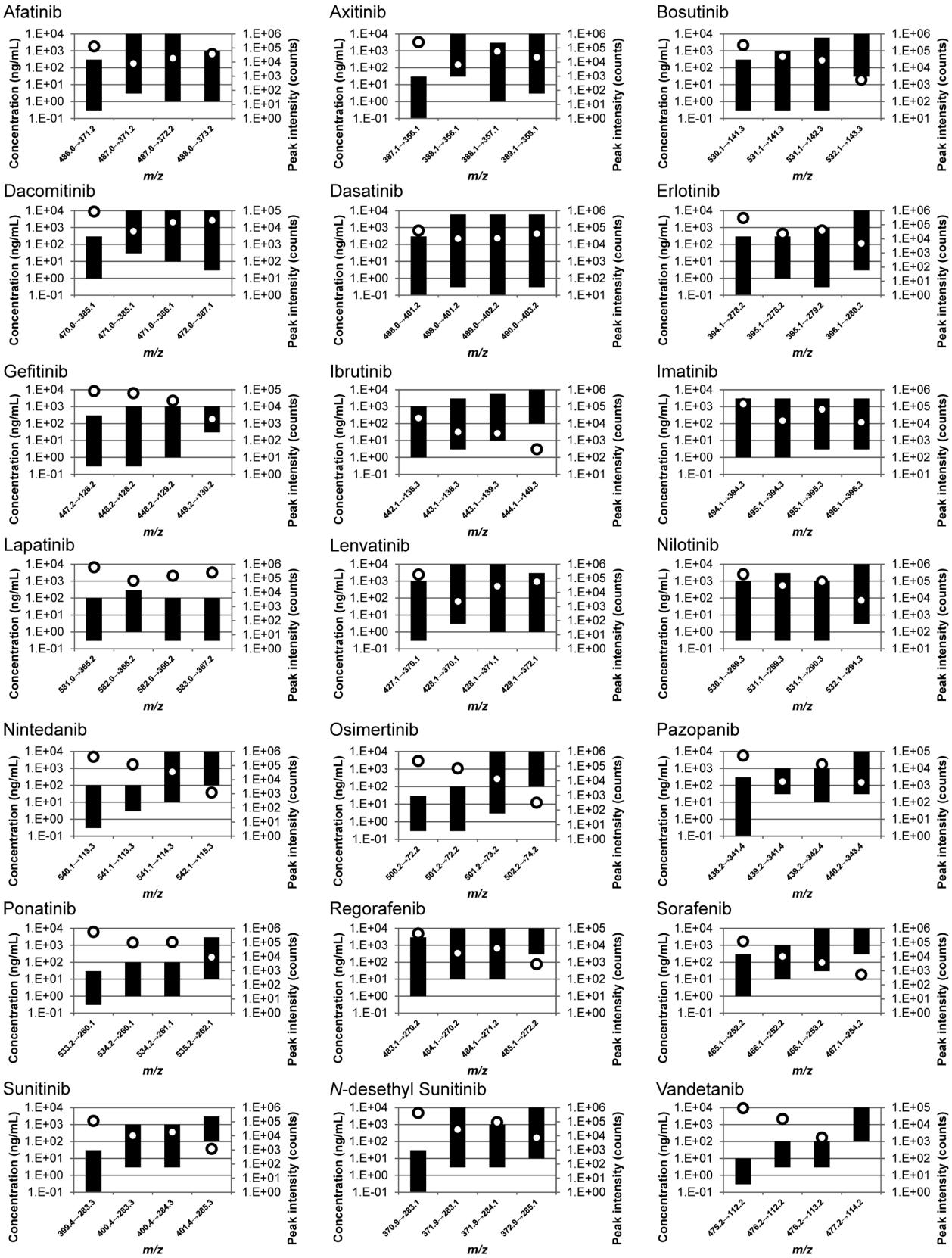

Fig. 6. Peak intensities plot and linearity range of calibration curves for optimized transitions and the isotopologue transition: afatinib, axitinib, bosutinib, dacomitinib, dasatinib, erlotinib, gefitinib, ibrutinib, imatinib, lapatinib, lenvatinib, nilotinib, nintedanib, osimertinib, pazopanib, ponatinib, regorafenib, sorafenib, sunitinib, *N*-desethyl sunitinib, and vandetanib.
The columns represent the linear range of the calibration curve (left *y*-axis). The white dots represent the change in peak intensities of each 10 pg analyte (right *y*-axis). When the peak intensity was not obtained, the white dot was not described.

decreased compared to the optimized transitions *m/z* 581.0 ＞365.2, and 493.1＞394.3, and no significant shift was observed in the linearity of the calibration curves (Fig. 6 and Table 2).

Considering these results, *i*-SRM can be used for most analytes because it is easy to predict changes in the peak intensities from the isotope abundance ratio. On the contrary, *i*-SRM was considered to be less effective in atomic compositions such as lapatinib ($C_{29}H_{26}ClFN_4O_4S$) and imatinib ($C_{29}H_{31}N_7O$). Lapatinib, in particular, was not affected by *i*-SRM because it contains Cl atoms in the structure of product ions and has a high natural abundance ratio, even in *m/z* M_1+2＞M_3+2 (*m/z* 583.0＞367.2). Furthermore, the effect of stable isotopes (^{2}H) is shown by overlapping peaks (similar *m/z* ions) from the same/similar retention times. It is necessary to investigate the possibility of affecting quantification depending on the compound.

Conclusion

In this study, we investigated the linear range shifts of the calibration curve by adjusting the CED, in-source CID, *s*-SRM, and *i*-SRM for 20 oral kinase inhibitors and the active metabolite of sunitinib. It was found that although these four techniques can easily adjust the number of ions in MS for many analytes, it is difficult to adapt 21 analytes using only one technique. Therefore, to develop a method for the simultaneous quantification of oral kinase inhibitors and the active metabolite in molecular-targeted therapy, it is important to utilize multiple techniques considering the therapeutic concentration range of each drug.

Acknowledgments

This work was supported by JSPS KAKENHI (grant number JP21K06708). We would like to thank Editage (www.editage.com) for the English language editing.

Conflict of Interest

The authors declare no conflicts of interest associated with this manuscript.

References

1) Hochhaus A, Baccarani M, Silver RT, Schiffer C, Apperley JF, et al: European LeukemiaNet 2020 recommendations for treating chronic myeloid leukemia. *Leukemia* 34: 966−984, 2020.
2) Roskoski R: Small molecule inhibitors targeting the EGFR/ErbB family of protein-tyrosine kinases in human cancers. *Pharmacol Res* 139: 395−411, 2019.
3) Mueller-Schoell A, Groenland SL, Scherf-Clavel O, van Dyk M, Huisinga W, et al: Therapeutic drug monitoring of oral targeted antineoplastic drugs. *Eur J Clin Pharmacol* 77: 441−464, 2021.
4) Verheijen RB, Yu H, Schellens JHM, Beijnen JH, Steeghs N, et al: Practical recommendations for therapeutic drug monitoring of kinase inhibitors in oncology. *Clin Pharmacol Ther* 102: 765−776, 2017.
5) Takasaki S, Kikuchi M, Kawasaki Y, Ito A, Arai Y, et al: A case of renal cell carcinoma with high everolimus blood concentrations and hyperglycemia due to everolimus-induced hepatic dysfunction. *Gan To Kagaku Ryoho* 44: 87−89, 2017.
6) Takasaki S, Kikuchi M, Kawasaki Y, Ito A, Arai Y, et al: Severe toxicity induced by accumulation of active sunitinib metabolite in a Japanese patient with renal cell carcinoma: A case report. *J Med Case Rep* 11: 28, 2017.
7) Takasaki S, Kawasaki Y, Kikuchi M, Tanaka M, Suzuka M, et al: Relationships between sunitinib plasma concentration and clinical outcomes in Japanese patients with metastatic renal cell carcinoma. *Int J Clin Oncol* 23: 936−943, 2018.
8) Yamaguchi H, Takasaki S, Kikuchi M, Kawasaki Y, Arai Y, et al: Toward personalized cancer therapy with oral molecular-targeted agents. *Yakugaku Zasshi* 139: 911−915, 2019.
9) Takasaki S, Adachi H, Kawasaki Y, Kikuchi M, Ito A, et al: Importance of therapeutic drug monitoring to detect drug interaction between pazopanib and warfarin: A case report. *J Pharm Pharm Sci* 23: 200−205, 2020.
10) Takasaki S, Kawasaki Y, Kikuchi M, Ito A, Yamaguchi H, et al: Clinical importance of blood drug concentration of oral molecular targeted drugs for renal cell carcinoma. *J Pharm Pharm Sci* 24: 127−136, 2021.
11) Takasaki S, Tanaka M, Kikuchi M, Maekawa M, Kawasaki Y, et al: Simultaneous analysis of oral anticancer drugs for renal cell carcinoma in human plasma using liquid chromatography/electrospray ionization tandem mass spectrometry. *Biomed Chromatogr* 32: e4184, 2018.
12) Sato Y, Shigeta K, Hirasawa T, Sato T, Ogura J, et al: Establishment of an analytical method for simultaneous quantitation of CDK4/6 inhibitors, aromatase inhibitors, and an estrogen receptor antagonist in human plasma using LC-ESI-MS/MS. *J Chromatogr B Analyt Technol*

Biomed Life Sci 1173: 122655, 2021.

13) Hirasawa T, Kikuchi M, Shigeta K, Takasaki S, Sato Y, et al: High-throughput liquid chromatography/electrospray ionization−tandem mass spectrometry method using in-source collision-induced dissociation for simultaneous quantification of imatinib, dasatinib, bosutinib, nilotinib, and ibrutinib in human plasma. *Biomed Chromatogr* 35: e5124, 2021.
14) Ishii H, Yamaguchi H, Mano N: Shifting the linear range in electrospray ionization by in-source collision-induced dissociation. *Chem Pharm Bull* 64: 356−359, 2016.
15) Ishii H, Shimada M, Yamaguchi H, Mano N: A simultaneous determination method for 5-fluorouracil and its metabolites in human plasma with linear range adjusted by in-source collision-induced dissociation using hydrophilic interaction liquid chromatography-electrospray ionization-tandem mass spectrometry. *Biomed Chromatogr* 30: 1882−1886, 2016.
16) Ishii H, Yamaguchi H, Mano N: Expanding the versatility of a quantitative determination range adjustment technique using in-source CID in LC/MS/MS. *Chromatography* 38: 59−63, 2017.
17) Maekawa M, Tsukamoto T, Takasaki S, Kikuchi M, Sato Y, et al: Fundamental study of behaviors of in-source collision induced dissociation and shifting the linear range of calibration curves of various drugs and the metabolites used for therapeutic drug monitoring. *Chromatography* 40: 71−78, 2019.
18) Sato T, Suzuka M, Sato Y, Iwabuchi R, Kobayashi D, et al: Development of a simultaneous analytical method for clozapine and its metabolites in human plasma using liquid chromatography/electrospray ionization tandem mass spectrometry with linear range adjusted by in-source collision-induced dissociation. *Biomed Chromatogr* 35, e5094, 2021.
19) Shen J, Wang H, Huang H, Li H, Li C, et al: Absolute quantitative analysis of endogenous neurotransmitters and amino acids by liquid chromatography-tandem mass spectrometry combined with multidimensional adsorption and collision energy defect. *J Chromatogr A* 1638: 461867, 2021.
20) Curtis MA, Matassa LC, Demers R, Fegan K: Expanding the linear dynamic range in quantitative high performance liquid chromatography/tandem mass spectrometry by the use of multiple product ions. *Rapid Commun Mass Spectrom* 15: 963−968, 2001.
21) Liu H, Lam L, Dasgupta PK: Expanding the linear dynamic range for multiple reaction monitoring in quantitative liquid chromatography-tandem mass spectrometry utilizing natural isotopologue transitions. *Talanta* 87: 307−310, 2011a.